Chemical Science

ROYAL SOCIETY OF CHEMISTRY

EDGE ARTICLE

View Article Online
View Journal | View Issue

Cite this: *Chem. Sci.*, 2025, **16**, 22348

All publication charges for this article have been paid for by the Royal Society of Chemistry

Received 4th September 2025
Accepted 6th October 2025

DOI: 10.1039/d5sc06836c

rsc.li/chemical-science

Fluorine-mediated single-step ethylene purification in face-transitive metal–organic frameworks from binary to ternary gas mixtures

Wei-Hong Zhang, Ya-Nan Ma, Guo-Tong Du, Ping Wang and Dong-Xu Xue *

Ethylene is a pivotal feedstock for the chemical industry. Obtaining polymer-grade ethylene in a single step from either binary ethane/ethylene or ternary acetylene/ethane/ethylene mixtures *via* porous adsorbents is highly energy-efficient yet remains a formidable challenge. Face-transitive topologies, a particular class of nets in reticular chemistry, possess only one window type and thus hold exceptional promise for discriminating between closely related C_2 hydrocarbons. Guided by the **nia-d** topology, we synthesized two isoreticular, trinuclear-manganese-cluster-based, ternary metal–organic frameworks (MOFs), namely **nia-d**-TZB and **nia-d**-FTZB, under solvothermal conditions using $MnCl_2$, the tritopic linker 2,4,6-tri(4-pyridyl)-1,3,5-triazine (TPT), and the heterofunctional linear linkers 4-(1*H*-tetrazol-5-yl)benzoic acid (H_2TZB) or 2-fluoro-4-(1*H*-tetrazol-5-yl)benzoic acid (H_2FTZB). Although the resultant trigonal-bipyramidal cages remain dimensionally invariant, the introduction of fluorine in the latter linker subtly reduces the size of the antiprismatic cages and the sole triangular window in **nia-d**-FTZB. Single-component adsorption isotherms reveal that **nia-d**-TZB preferentially adsorbs ethane, whereas **nia-d**-FTZB preferentially adsorbs both acetylene and ethane. Consequently, **nia-d**-TZB enables one-step purification of ethylene from an ethane/ethylene mixture, while **nia-d**-FTZB achieves simultaneous removal of acetylene and ethane from an acetylene/ethane/ethylene ternary stream, again delivering polymer-grade ethylene in a single pass. These findings are corroborated by ideal adsorbed solution theory (IAST), breakthrough experiments with both binary and ternary gas mixtures, and detailed theoretical simulations. This study furnishes compelling evidence for the rational design of face-transitive MOFs to tackle complex gas-separation tasks.

Introduction

Ethylene (C_2H_4), a cornerstone of the modern petrochemical industry with an annual global production exceeding 200 million tons, serves as the primary feedstock for polyethylene and other commodity chemicals. Currently, industrial C_2H_4 production relies on the processes such as naphtha steam cracking and ethane dehydrogenation, which inevitably generate by-products like acetylene (C_2H_2) and ethane (C_2H_6). Achieving polymer-grade ethylene (purity > 99.9%) demands complete removal of these impurities. Conventional purification employs a multi-step approach: selective hydrogenation of C_2H_2 using noble-metal catalysts (*e.g.*, Pd) followed by cryogenic distillation to separate C_2H_4/C_2H_6.[1–4] However, this process suffers from excessive energy consumption (distillation operates at high pressure and subzero temperatures) and environmental burdens. The challenge is further exacerbated by the overlapping boiling points (184.6 K, 188.4 K, and 169.4 K for C_2H_6, C_2H_2, and C_2H_4, respectively), rendering traditional separation methods inefficient. Adsorptive separation employing porous materials offers a highly promising, energy-efficient alternative to conventional methods.[5]

Metal–organic frameworks (MOFs), as a class of emerging crystalline porous materials, have attracted intensive attention from the scientific community to industry over the past two decades.[6–10] These materials combine facile synthesis, well-defined structures, tunable functionalities, and rich chemical diversity, endowing them with broad potential across gas storage,[11–18] separation,[19–24] catalysis,[25–29] sensing,[30–36] pharmaceutical delivery[37,38] and so on. In particular, MOFs have achieved notable progress in ethylene purification. Current reports on ethylene purification primarily address binary gas separations, namely ethylene/acetylene and ethylene/ethane mixtures, as well as trinary gas separations, *i.e.*, ethylene/acetylene/ethane mixtures.[39–44] In binary ethylene/ethane separations, ethane-selective adsorbents have garnered considerable interest in recent years because they enable direct, single-step ethylene purification with reduced energy expenditure by avoiding secondary desorption steps.[45,46] Given that the kinetic

---

Shaanxi Provincial Key Laboratory of New Concept Sensors and Molecular Materials, Key Laboratory of Applied Surface and Colloid Chemistry of Ministry of Education, School of Chemistry & Chemical Engineering, Shaanxi Normal University, Xi'an 710119, China. E-mail: xuedx@snnu.edu.cn

diameters, the quadrupole moment and polarizability of ethylene (C_2H_4: 4.16 Å, approximately 1.5×10^{-26} esu cm^2 and 42.5×10^{-25} cm^3, respectively) lie between those of acetylene (C_2H_2: 3.33 Å, 7.2×10^{-26} esu cm^2 and 39.3×10^{-25} cm^3, respectively) and ethane (C_2H_6: 4.44 Å, 0.65×10^{-26} esu cm^2 and 44.7×10^{-25} cm^3, respectively), achieving simultaneous removal of acetylene and ethane from a C_2 mixture to yield one-step ethylene purification from the three-component ethylene/acetylene/ethane feed remains exceptionally challenging.[47] In recent years, numerous MOF materials have been reported that enable one-step purification of ethylene from both two-component[48–56] and three-component C_2 mixtures.[57–64] Nevertheless, the design and synthesis of new MOFs that combine high selectivity with large uptake remains highly anticipated within the community.

Topology-guided reticular chemistry plays a crucial role in the design and synthesis of MOFs.[65–68] In particular, MOF networks with a single window are referred to as face-transitive.[69] The window serves as the sole gateway for gas molecules to enter and exit the internal cavities. Consequently, structures featuring only a single window are more readily tunable during bottom-up assembly. As a result, the regulated synthesis of face-transitive MOFs has emerged as an effective strategy to address efficient gas separations. Among them, **nia-d**, also known as **pacs**, is a (3,9)-c topology with a transitivity of 2212.[70] This notation indicates that the network contains two kinds of vertices, two kinds of edges, one kind of face (window), and two kinds of tiles (cavities), thereby constituting a face-transitive network. In recent years, **nia-d**/**pacs**-type network has attracted considerable attention from numerous research groups for its potential in guiding high-performance gas separation MOFs.[71–77]

Building on the above findings and the isoreticular chemistry strategy, we report the synthesis of two **nia-d**-type trinuclear manganese-based MOFs using the same metal source and a tridentate triazine ligand, as well as a hetero-functional linear linker bearing carboxylic acid and tetrazole motifs. One linker is fluorine-free, while the side arm of the carboxylate in the other linker is fluorinated. Notably, these two materials exhibit distinct adsorption behaviours toward C_2 hydrocarbons, leading to different separation performances. The synthesis and structure, as well as the adsorption and separation properties, breakthrough measurements with mixed C_2 feeds, and mechanistic interpretations, are described in detail below.

Results and discussion

Synthesis and structure

Indeed, solvothermal reactions at 135 °C in DMF solvent combining $MnCl_2$ with 2,4,6-tri(4-pyridyl)-1,3,5-triazine (TPT) and either 4-(1*H*-tetrazol-5-yl)benzoic acid (H_2TZB) or 2-fluoro-4-(1*H*-tetrazol-5-yl)benzoic acid (H_2FTZB) with trifluoroacetic acid as additive yielded yellow hexagonal-prismatic single crystals. Single-crystal X-ray diffraction (SCXRD), together with dye exchange experiments and X-ray photoelectron spectroscopy (XPS) (Fig. S3–S6), established the molecular formulae as $[Mn^{II}Mn^{III}_2(\mu_3\text{-}O)(TZB)_3TPT]\cdot x$(solvent) for **nia-d**-TZB and $[Mn^{II}Mn^{III}_2(\mu_3\text{-}O)(FTZB)_3TPT]\cdot x$(solvent) for **nia-d**-FTZB. SCXRD reveals that **nia-d**-TZB and **nia-d**-FTZB are isoreticular (Tables S4 and S5), both crystallizing in the hexagonal space group *P*6$_3$/*mmc*. In both structures, linear linkers yield the well-known 6-c **acs** network. The hexagonal channels are then sequentially occupied by triangular TPT linkers that cap the exposed $[Mn_3(\mu_3\text{-}O)]$ clusters, leading to the intended (3,9)-c **nia-d** topological 3-periodic framework.

Two distinct cage motifs are present in both compounds, *i.e.*, a triangular bipyramidal cage (cage-I) and an anti-prismatic cage (cage-II). The dimensions of cage-I are 9.96×16.15 Å^2 in both structures. The presence of fluorine in the linear linker slightly perturbs cage-II, changing its dimensions from 13.17×6.30 Å^2 in **nia-d**-TZB to 12.62×6.23 Å^2 in **nia-d**-FTZB (Fig. 1). At the same time, the triangular windows, defined by portions of the TPT linker and two linear linkers, serve as the sole entrances/exits for the framework. The aperture size modestly decreases from 5.16 Å in **nia-d**-TZB to 5.0 Å in **nia-d**-FTZB (Fig. S2). Nevertheless, these window dimensions remain sufficient to permit the passage of C_2 gas molecules.

Porosity, adsorption and separation

The solvent-accessible pore volumes for **nia-d**-TZB and **nia-d**-FTZB are 57.9% and 54.2%, respectively. The excellent agreement between bulk powder X-ray diffraction (PXRD) patterns and single-crystal simulations confirms the phase purity of the synthesized materials (Fig. S12 and S13). To assess porosity, the two samples were subjected to three days of consecutive exchanges with acetonitrile or acetone, followed by evacuation at 120 °C under vacuum prior to adsorption measurements. Nitrogen sorption isotherms measured at 77 K display Type-I behaviour for both samples, consistent with their microporous character. At 1 bar, **nia-d**-TZB (546 cm^3 g^{-1}) exhibits a higher nitrogen uptake than **nia-d**-FTZB (503 cm^3 g^{-1}) (Fig. 2 and S7). Correspondingly, the BET surface areas and pore volumes are 2029 m^2 g^{-1} and 0.85 cm^3 g^{-1}, respectively, for **nia-d**-TZB, and 1987 m^2 g^{-1} and 0.78 cm^3 g^{-1}, respectively, for **nia-d**-FTZB, which are consistent with their respective theoretical pore volumes of 0.85 cm^3 g^{-1} and 0.77 cm^3 g^{-1}, thereby confirming that the materials were fully activated. The pore size distributions are centered at 11.5 Å and 11.0 Å, respectively (Fig. S8). These results are in good agreement with the pore architectures inferred from the single-crystal structures, indicating that both materials were successfully activated and preserved their structural integrity.

To probe the C_2 gas adsorption behaviour, we collected a series of static sorption isotherms for **nia-d**-TZB and **nia-d**-FTZB. As shown in Fig. 3a, both materials exhibit higher uptake for ethane and acetylene than for ethylene. Specifically, at 298 K and 1 bar, the uptakes are 143.72 cm^3 g^{-1} for C_2H_6, 124.46 cm^3 g^{-1} for C_2H_2, and 107.42 cm^3 g^{-1} for C_2H_4 in **nia-d**-TZB. These uptakes are consistent with the zero-coverage isosteric heats of adsorption (Q_{st}), *i.e.*, 29.85 kJ mol^{-1} (C_2H_6), 27.88 kJ mol^{-1} (C_2H_2), and 26.19 kJ mol^{-1} (C_2H_4) (Fig. 3c and S16). Notably, the ethane uptake for **nia-d**-TZB reaches 6.42 mmol g^{-1}, a value higher than those of many benchmark ethane-selective

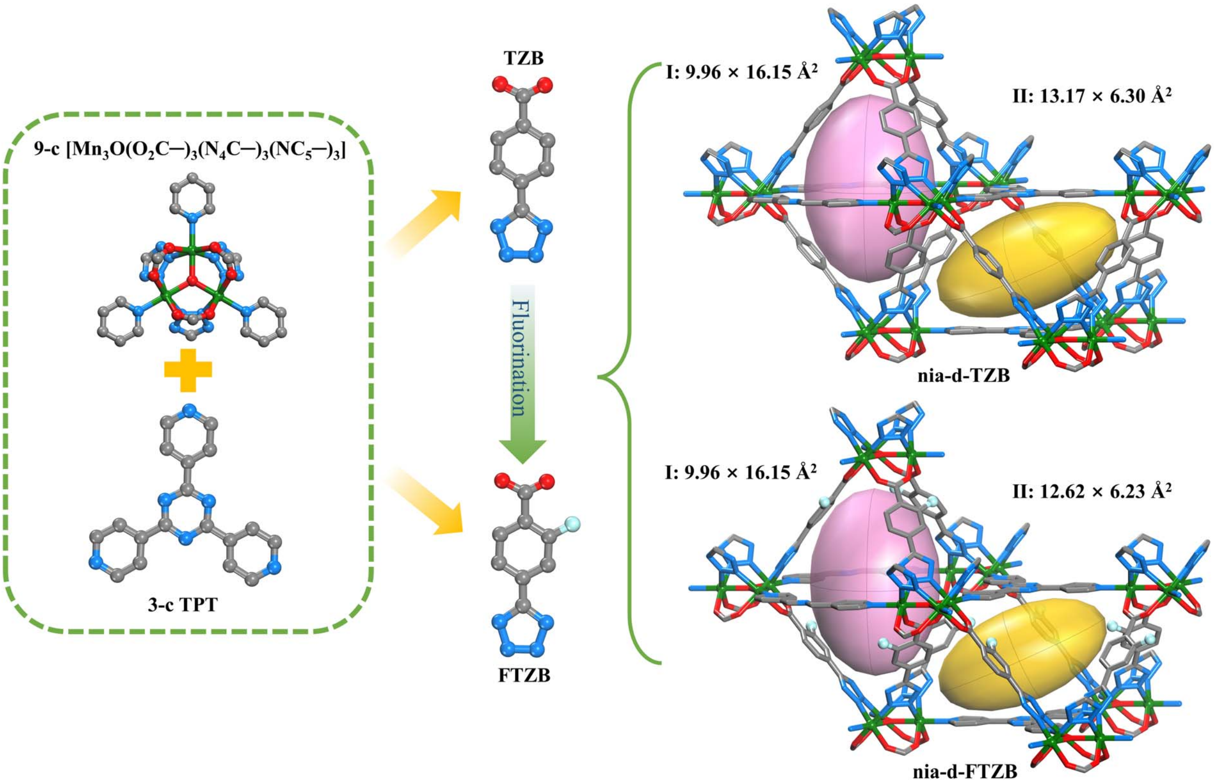

Fig. 1 Schematic representation of the two MOFs constructed from a trinuclear manganese cluster and respective mixed linkers associated with corresponding cage sizes. C: gray, Mn: green, O: red, N: sky blue, and F: light blue. Hydrogen atoms are omitted for clarity.

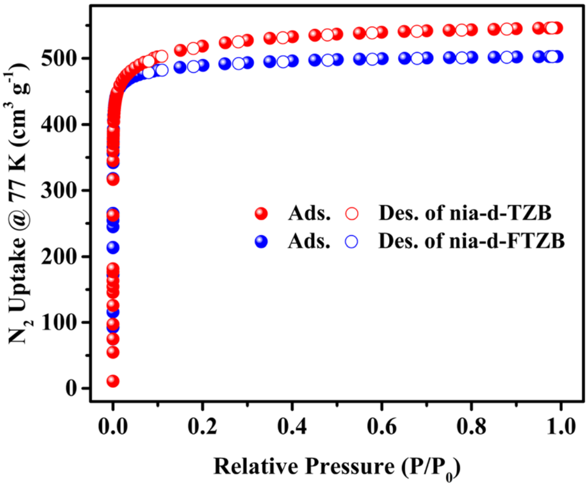

Fig. 2 The N_2 sorption isotherms at 77 K for **nia-d**-TZB and **nia-d**-FTZB.

adsorbents, such as PCN-250 (5.21 mmol g^{-1}),[78] Ni-MOF-2 (5.94 mmol g^{-1}),[55] MOF-303 (5.01 mmol g^{-1}),[79] and UiO-67-$(NH_2)_2$ (5.32 mmol g^{-1}).[80] The C_2H_6/C_2H_4 and C_2H_2/C_2H_4 uptake ratios are 1.34 and 1.16, respectively. It is noteworthy that the adsorption isotherms for C_2H_2 and C_2H_4 are very close at low pressure, and the C_2H_2/C_2H_4 uptake ratio is relatively low. Collectively, **nia-d**-TZB demonstrates a pronounced ethane-selective adsorption behaviour toward C_2 gas mixtures, which is advantageous for the removal of ethane from binary C_2H_6/C_2H_4 feeds and enables one-step purification of ethylene.

As for **nia-d**-FTZB, the introduction of fluorine markedly alters its adsorption profile, yielding the highest uptake for acetylene among the C_2 molecules studied. Specifically, at 298 K and 1 bar, the uptakes are 162.98 cm^3 g^{-1} for C_2H_2, 140.94 cm^3 g^{-1} for C_2H_6, and 125.69 cm^3 g^{-1} for C_2H_4 (Fig. 3b). The corresponding zero-coverage Q_{st} is 29.98 kJ mol^{-1} (C_2H_2), 29.53 kJ mol^{-1} (C_2H_6), and 27.95 kJ mol^{-1} (C_2H_4) (Fig. 3c and S17). The ethane uptake remains notably high, and although the ethylene uptake also increases, the C_2H_2 isotherm lies above the C_2H_4 isotherm within 0–1.0 bar. The C_2H_2/C_2H_4 uptake ratio increases to 1.30. These data indicate that **nia-d**-FTZB exhibits concurrent selective adsorption of both acetylene and ethane, suggesting its potential for simultaneous removal of C_2H_2 and C_2H_6 from ternary C_2 feeds and enabling one-step purification of ethylene.

To assess the gas separation performance of **nia-d**-TZB and **nia-d**-FTZB, we calculated the selectivities for binary mixtures of C_2H_2/C_2H_4 and C_2H_6/C_2H_4 using ideal adsorbed solution theory (IAST) (Fig. S20–S22). At 298 K and 1 bar, the selectivities for the C_2H_2/C_2H_4 (50/50, v/v) mixtures are 1.11 for **nia-d**-TZB and 1.45 for **nia-d**-FTZB (Fig. 3d). Under the same conditions, the selectivities for the C_2H_6/C_2H_4 (50/50, 10/90, v/v) mixture are 1.58 for **nia-d**-TZB and 1.41 for **nia-d**-FTZB (Fig. 3d). These values are comparable to those of many benchmark ethane-selective

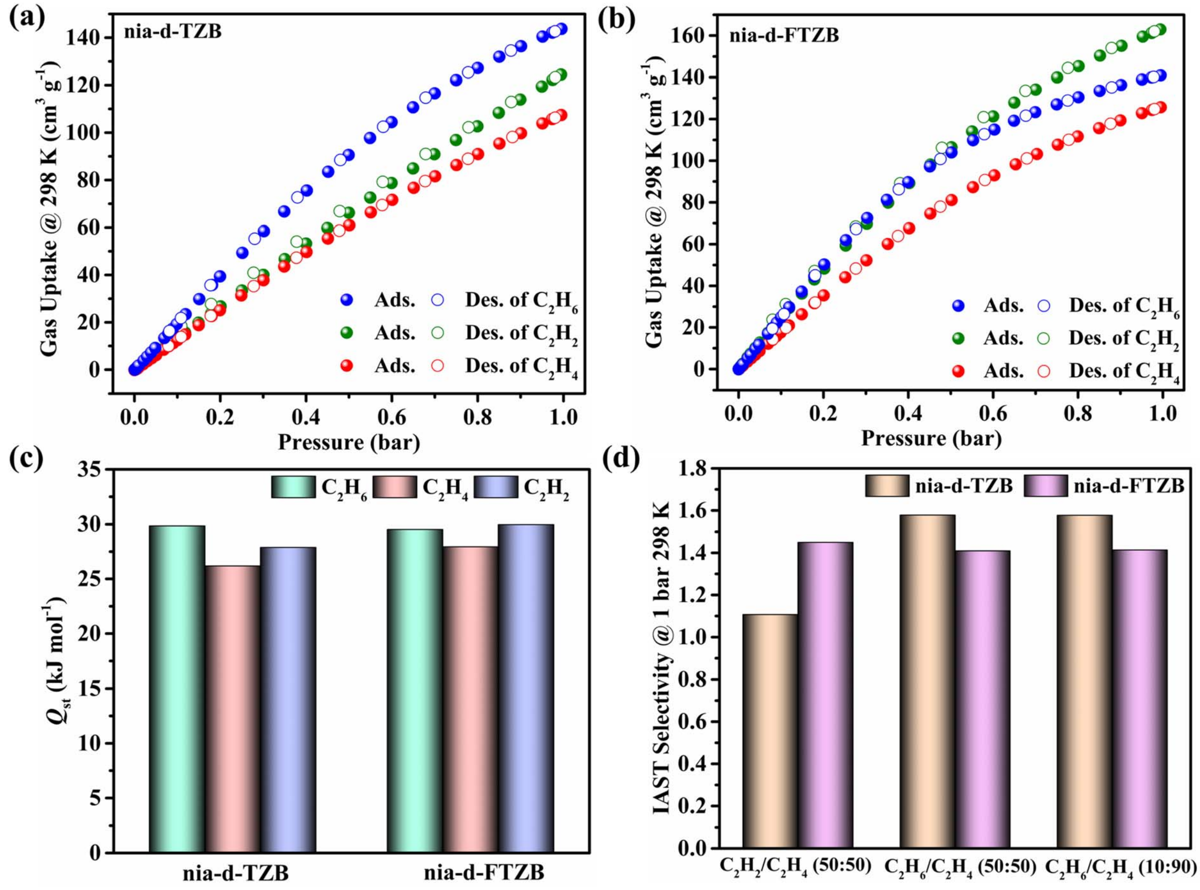

Fig. 3 (a) C_2H_2, C_2H_6, and C_2H_4 sorption isotherms of **nia-d**-TZB at 298 K; (b) C_2 sorption isotherms of **nia-d**-FTZB at 298 K; (c) Q_{st} of C_2H_2, C_2H_6 and C_2H_4 for **nia-d**-TZB and **nia-d**-FTZB; (d) IAST selectivity of **nia-d**-TZB and **nia-d**-FTZB for C_2H_2/C_2H_4 (50/50, v/v) and C_2H_6/C_2H_4 (50/50, 10/90, v/v) at 298 K and 1 bar.

MOFs, such as Azole-Th-1 (1.46),[57] Zn-atz-oba (1.27),[81] JNU-2 (1.6),[82] and BF-108-Zn (1.37).[83] The results align with the observation that **nia-d**-TZB favors ethane removal from binary ethane/ethylene feeds, while **nia-d**-FTZB shows promise for simultaneous removal of acetylene and ethane from ternary C_2 mixtures, enabling one-step ethylene purification.

Breakthrough experiment

To evaluate the practical separation performance, fixed-bed breakthrough experiments were performed with the samples activated at 120 °C. For **nia-d**-TZB, we first tested the binary C_2H_2/C_2H_4 (50/50, v/v) and ternary $C_2H_2/C_2H_6/C_2H_4$ (1/1/1, v/v/v) mixtures at 298 K and 1 bar with a total flow rate of 1.0 mL min^{-1}. In two configurations, both C_2H_2 and C_2H_4 were observed at the outlet, indicating that no effective separation of the two components could be achieved under these conditions (Fig. 4a and S24). This result is consistent with the similar low-pressure isotherms for C_2H_2 and C_2H_4 and the modest difference in their adsorption affinities. In contrast, when the binary C_2H_6/C_2H_4 mixtures (50/50, v/v) at the total flow-rates of 1.0 mL min^{-1} were introduced into the fixed-bed, **nia-d**-TZB demonstrated a meaningful separation of C_2H_6 from C_2H_4 (Fig. 4b and S23). The breakthrough behaviour yielded a C_2H_6/C_2H_4 separation interval of about 6.4 min g^{-1}. Notably, with a 10/90 (v/v) C_2H_6/C_2H_4 feed and a flow rate of 1.0 mL min^{-1}, C_2H_4 began to emerge at the outlet around 78 min g^{-1}, followed by a slower C_2H_6 elution after ~19.1 min g^{-1} (Fig. 4c and S23). The observed performance rivals several established ethane-selective materials reported in the literature, *e.g.*, JNU-2 (16 min g^{-1}),[82] TKL-106 (15 min g^{-1}),[84] UPC-612 (11.5 min g^{-1}),[85] Zn-BPZ-TATB (14 min g^{-1}),[86] NUM-9 (16 min g^{-1}),[87] JNU-74 (22 min g^{-1}),[88] and MOF-801 (20 min g^{-1}).[89] The material demonstrated a C_2H_4 production capacity of 17.19 L kg^{-1}. These results demonstrate that **nia-d**-TZB can effectively separate C_2H_6 from C_2H_4 in binary feeds, enabling practical single-step ethylene purification from ethane-containing streams.

For **nia-d**-FTZB, breakthrough experiments were conducted similarly. In the binary C_2H_2/C_2H_4 (50/50, v/v) test with a 1.0 mL min^{-1} flow rate, C_2H_4 eluted prior to C_2H_2, with C_2H_4 breakthrough occurring at ~42 min g^{-1} and C_2H_2 subsequently reaching equilibrium after ~4.6 min g^{-1} (Fig. 4d and S26). This demonstrates effective separation of acetylene from ethylene in this binary gas pair. We also tested the binary C_2H_6/C_2H_4 (50/50, 10/90, v/v) feeds at 1.0 and 2.0 mL min^{-1}. **nia-d**-FTZB showed a measurable separation performance for these two gases, with a separation interval of roughly 7.9 min g^{-1} and 13.2 min g^{-1}

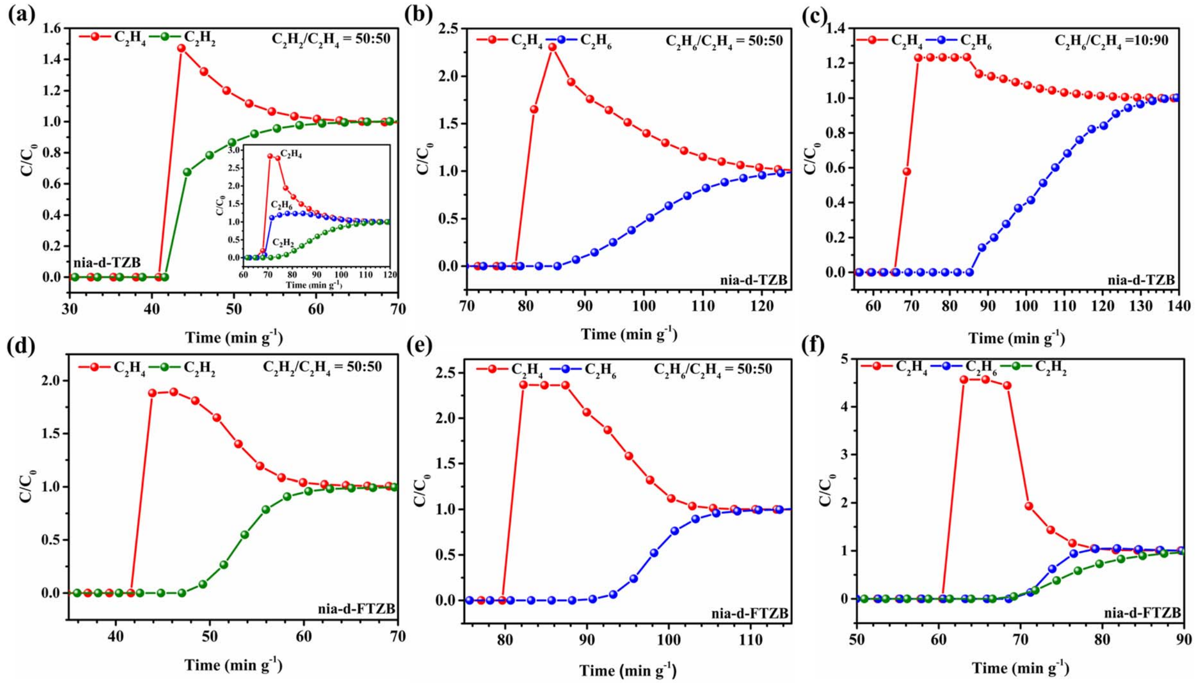

Fig. 4 Experimental breakthrough curves for **nia-d**-TZB at a total gas flow rate of 1.0 mL min^{-1} of (a) C_2H_2/C_2H_4 (50/50, v/v) and $C_2H_6/C_2H_4/C_2H_2$ (1/1/1, v/v/v), (b) C_2H_6/C_2H_4 (50/50, v/v) and (c) C_2H_6/C_2H_4 (10/90, v/v) at 298 K and 1 bar. Experimental breakthrough curves for **nia-d**-FTZB at a total gas flow rate of 1.0 mL min^{-1} of (d) C_2H_2/C_2H_4 (50/50, v/v), (e) C_2H_6/C_2H_4 (50/50, v/v) and (f) $C_2H_6/C_2H_4/C_2H_2$ (1/1/1, v/v/v) at 298 K and 1 bar.

observed. With a 10/90 (v/v) C_2H_6/C_2H_4 feed and a flow rate of 1.0 mL min^{-1}, the C_2H_4 productivity reached 11.88 L kg^{-1}, confirming its ability to discriminate between C_2H_6 and C_2H_4 under practical flow conditions (Fig. 4e, S25 and S26).

To probe the full potential for ternary gas mixture separation, fixed-bed breakthrough experiments were performed with a $C_2H_2/C_2H_6/C_2H_4$ (1/1/1, v/v/v) feed at 298 K and 1.0 mL min^{-1}. In this mixed-gas test, C_2H_4 was detected at the outlet first (*i.e.*, 61 min g^{-1}), followed by C_2H_6 (after 5.3 min g^{-1}), and finally C_2H_2, validating the potential for one-step ethylene purification in the presence of acetylene and ethane (Fig. 4f). The productivity of C_2H_4 separation from the ternary mixture after the elution of C_2H_2 and C_2H_6 can be 1.77 L kg^{-1}.

The materials demonstrate outstanding regenerability, retaining high separation performance over multiple breakthrough cycles. Regeneration does not require heating. It only needs to be purged with 10.0 mL min^{-1} helium gas at 298 K for 30 minutes. Both **nia-d**-TZB and **nia-d**-FTZB exhibit exceptional cycling stability without noticeable degradation in adsorption capacity or selectivity across five times repeated runs (Fig. S26).

GCMC simulation

To gain a deeper understanding of the selective adsorption and separation mechanism, modelling studies were conducted on **nia-d**-TZB and **nia-d**-FTZB using grand canonical Monte Carlo (GCMC) simulation. As illustrated in Fig. 5, the C_2 gases are located at different positions within the framework of **nia-d**-TZB. C_2H_2 and C_2H_4 molecules exhibit similar adsorption positions and interaction features. Both gases are predominantly distributed around the triangular windows, where C_2H_2 molecules form C–H$\cdots$N interactions with nitrogen atoms in the tetrazole rings or TPT, with distances ranging from 3.33 to 3.68 Å. Additionally, these molecules engage in C–H$\cdots\pi$ interactions with pyridine rings on the TPT ligands, with an average distance of 3.32 Å (Fig. 5a). Similarly, C_2H_4 molecules occupy comparable binding sites, primarily interacting with tetrazole nitrogen atoms, benzene ring and TPT *via* C–H$\cdots\pi$ and C–H$\cdots$N interactions, with distances ranging from 3.43 to 3.50 Å and 3.60–3.98 Å, respectively (Fig. 5b). In contrast, the distribution of C_2H_6 is distinct. These molecules are mainly localized at the metal cluster vertices, where they are surrounded by the framework, leading to stronger interactions. The primary binding sites for C_2H_6 involve interactions with carboxylate oxygen atoms through C–H$\cdots$O hydrogen bonds (distances of 3.01–3.70 Å) and with benzene rings *via* C–H$\cdots\pi$ interactions (distances of 3.21–3.95 Å) (Fig. 5c). The computational results indicate that **nia-d**-TZB exhibits stronger interactions with C_2H_6 than with C_2H_4 or C_2H_2, which aligns well with the experimental adsorption isotherms and the dynamic breakthrough results.

In contrast, all C_2 molecules are located at the metal cluster vertices of **nia-d**-FTZB. C_2H_2 and C_2H_6 display similar adsorption behaviours and binding sites. Specifically, C_2H_2 molecules form strong C–H$\cdots$F interactions with fluorine atoms on FTZB (distance: 2.71 Å), C–H$\cdots$O interactions with carboxylate oxygen (distance: 3.88 Å), C–H$\cdots$N interactions with tetrazole nitrogen atoms (distances: 2.94–3.85 Å), and C–H$\cdots\pi$ interactions with the tetrazole ring (distance: 3.32 Å) (Fig. 5d). C_2H_6 molecules also form multiple hydrogen bonds with fluorine atoms and

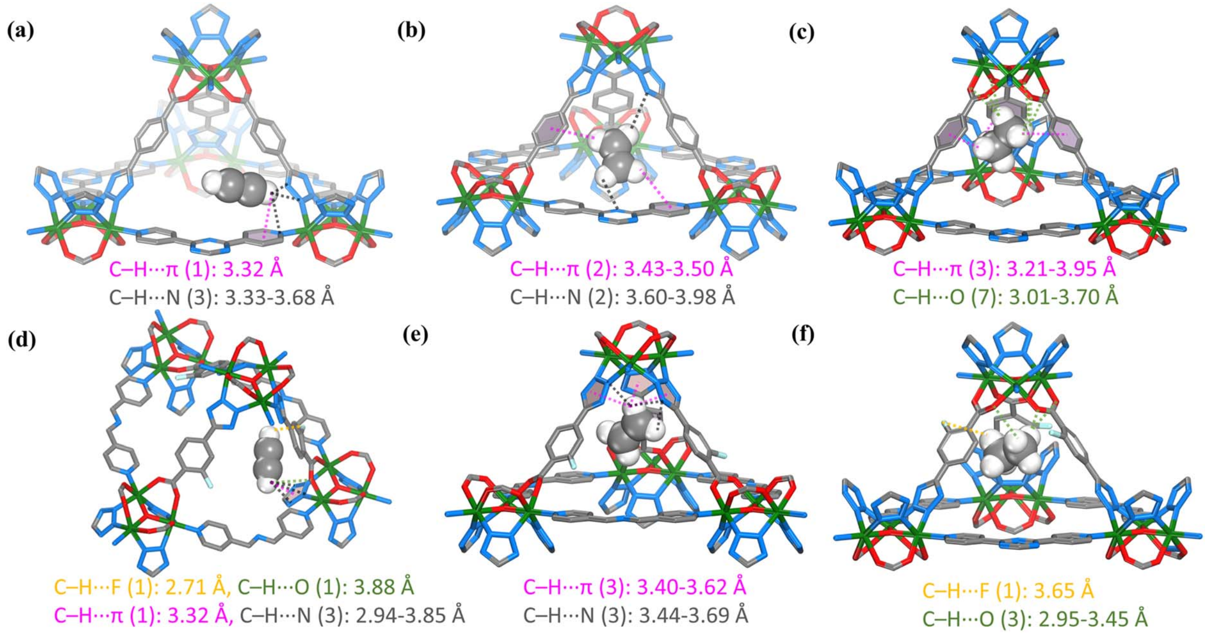

Fig. 5 The calculated preferential adsorption sites of **nia-d**-TZB for (a) C_2H_2, (b) C_2H_4 and (c) C_2H_6. The calculated preferential adsorption sites of **nia-d**-FTZB for (d) C_2H_2, (e) C_2H_4 and (f) C_2H_6. C: gray, Mn: green, O: red, N: sky blue, and F: light blue. The interactions are shown as dashed lines. For clarity, H atoms on frameworks are omitted.

carboxylate oxygen atoms, with interaction distances of C–H···F at 3.65 Å and C–H···O at 2.95–3.45 Å (Fig. 5f). The binding sites for C_2H_4 differ significantly. These molecules primarily interact with the surrounding three tetrazole rings, forming relatively weak C–H···π interactions with the tetrazole (distances: 3.40–3.62 Å) and multiple C–H···N interactions with tetrazole nitrogen atoms (distances: 3.44–3.69 Å) (Fig. 5e). The calculated binding energies follow the order: C_2H_2 (33.74 kJ mol^{-1}) > C_2H_6 (27.58 kJ mol^{-1}) > C_2H_4 (21.52 kJ mol^{-1}). These results indicate that **nia-d**-FTZB exhibits strong and comparable adsorption capacities for C_2H_2 and C_2H_6, with the strongest interaction observed for C_2H_2 and the weakest for C_2H_4, consistent with the adsorption results.

Overall, computational findings confirm that both **nia-d**-TZB and **nia-d**-FTZB possess the capability for reverse separation of C_2H_6/C_2H_4. The introduction of fluorine atoms on the linear linkers modifies the chemical microenvironment as well as the interaction sites, subsequently strengthening the interactions between guest molecules and the framework. Therefore, **nia-d**-FTZB demonstrates the potential not only for the reverse separation of the binary C_2H_6/C_2H_4 mixture, but also the one-step purification of C_2H_4 from ternary C_2 hydrocarbon mixtures.

Conclusions

Leveraging reticular chemistry and a mixed-ligand strategy, two isoreticular, trinuclear-manganese-cluster-based, ternary MOFs, designated as **nia-d**-TZB and **nia-d**-FTZB, have been successfully synthesized. Both frameworks adopt the **nia-d** topology, a face-transitive net that endows the structures with a single window type. The strategic installation of fluorine atoms along the linear linker transforms TZB into FTZB, which in turn elicits markedly divergent C_2-hydrocarbon sorption behaviours. In **nia-d**-TZB, acetylene and ethylene are taken up in comparable amounts, whereas ethane is adsorbed most strongly, enabling one-step ethylene purification from an ethane/ethylene binary mixture. In stark contrast, **nia-d**-FTZB exhibits the highest uptake for acetylene, followed by ethane, with ethylene being the least adsorbed. This hierarchy allows simultaneous removal of both acetylene and ethane from an acetylene/ethane/ethylene ternary stream, again delivering polymer-grade ethylene in a single step. Collectively, this work establishes a critical paradigm for the deliberate design of face-transitive MOFs that achieve advanced gas-separation performance, underscoring the potential of crystalline porous materials to contribute to energy savings and emission reductions.

Author contributions

Wei-Hong Zhang: writing – original draft, supervision; Ya-Nan Ma: analysis of the single crystal structure; Guo-Tong Du: computational analysis; Ping Wang: performed a part of characterization of MOF materials; Dong-Xu Xue: writing – review & editing, supervision, data curation.

Conflicts of interest

There are no conflicts to declare.

Data availability

CCDC 2482490 and 2482491 contain the supplementary crystallographic data for this paper.[90a,b]

All experimental supporting data and procedures are available in the supplementary information (SI). Supplementary information is available. See DOI: **https://doi.org/10.1039/d5sc06836c**.

Acknowledgements

We gratefully acknowledge the National Natural Science Foundation of China (No. 22471148 and 21871170), the National Key Research and Development Program of China (No. 2022YFA1205502), the Fundamental Research Funds for the Central Universities (No. GK202505027), and the Thousand Talents Program of Shaanxi Province and the Youth Innovation Team of Shaanxi Universities (2023).

Notes and references

1 S. Chu, Y. Cui and N. Liu, *Nat. Mater.*, 2016, **16**, 16–22.
2 S. M. Sadrameli, *Fuel*, 2016, **173**, 285–297.
3 I. Amghizar, L. A. Vandewalle, K. M. Van Geem and G. B. Marin, *Engineering*, 2017, **3**, 171–178.
4 S. A. Chernyak, M. Corda, J. P. Dath, V. V. Ordomsky and A. Y. Khodakov, *Chem. Soc. Rev.*, 2022, **51**, 7994–8044.
5 D. S. Sholl and R. P. Lively, *Nature*, 2016, **532**, 435–437.
6 S. L. James, *Chem. Soc. Rev.*, 2003, **32**, 276–288.
7 J. R. Long and O. M. Yaghi, *Chem. Soc. Rev.*, 2009, **38**, 1213–1214.
8 B. Li, H. M. Wen, Y. Cui, W. Zhou, G. Qian and B. Chen, *Adv. Mater.*, 2016, **28**, 8819–8860.
9 H. C. Zhou and S. Kitagawa, *Chem. Soc. Rev.*, 2014, **43**, 5415–5418.
10 H. C. Zhou, J. R. Long and O. M. Yaghi, *Chem. Rev.*, 2012, **112**, 673–674.
11 Y. He, W. Zhou, T. Yildirim and B. Chen, *Energy Environ. Sci.*, 2013, **6**, 2735–2744.
12 K. G. Froudas, M. Vassaki, K. Papadopoulos, C. Tsangarakis, X. Chen, W. Shepard, D. Fairen-Jimenez, C. Tampaxis, G. Charalambopoulou, T. A. Steriotis and P. N. Trikalitis, *J. Am. Chem. Soc.*, 2024, **146**, 8961–8970.
13 L. Liang, C. Liu, F. Jiang, Q. Chen, L. Zhang, H. Xue, H. L. Jiang, J. Qian, D. Yuan and M. Hong, *Nat. Commun.*, 2017, **8**, 1233.
14 D. Sengupta, P. Melix, S. Bose, J. Duncan, X. Wang, M. R. Mian, K. O. Kirlikovali, F. Joodaki, T. Islamoglu, T. Yildirim, R. Q. Snurr and O. K. Farha, *J. Am. Chem. Soc.*, 2023, **145**, 20492–20502.
15 J. Zhou, Y. N. Ma, Y. F. Zhang, B. Zheng, K. Zheng, S. Liu, X. A. Guo, Y. B. Zhang and D. X. Xue, *J. Am. Chem. Soc.*, 2025, **147**, 21811–21817.
16 Y. Yabuuchi, H. Furukawa, K. M. Carsch, R. A. Klein, N. V. Tkachenko, A. J. Huang, Y. Cheng, K. M. Taddei, E. Novak, C. M. Brown, M. Head-Gordon and J. R. Long, *J. Am. Chem. Soc.*, 2024, **146**, 22759–22776.
17 R. C. Rohde, K. M. Carsch, M. N. Dods, H. Z. H. Jiang, A. R. McIsaac, R. A. Klein, H. Kwon, S. L. Karstens, Y. Wang, A. J. Huang, J. W. Taylor, Y. Yabuuchi, N. V. Tkachenko, K. R. Meihaus, H. Furukawa, D. R. Yahne, K. E. Engler, K. C. Bustillo, A. M. Minor, J. A. Reimer, M. Head-Gordon, C. M. Brown and J. R. Long, *Science*, 2024, **386**, 814–819.
18 S. Lu, Y.-J. Zhang, Y.-J. Cheng, Z.-H. Qin, G.-D. Wang, Y. Bai, Y. Lin, H. Wang, Y. Sui, L. Hou and Y.-Z. Li, *J. Mater. Chem. A*, 2025, **13**, 10581–10589.
19 Y. Ding, A. Dey, L. O. Alimi, P. M. Bhatt, J. Du, C. Maaliki, M. Eddaoudi, J. Jacquemin and N. M. Khashab, *Chem. Mater.*, 2021, **34**, 197–202.
20 M. Chang, F. Wang, Y. Wei, Q. Yang, J. X. Wang, D. Liu and J. F. Chen, *AIChE J.*, 2022, **68**, e17794.
21 K. B. Idrees, Z. Li, H. Xie, K. O. Kirlikovali, M. Kazem-Rostami, X. Wang, X. Wang, T. Y. Tai, T. Islamoglu, J. F. Stoddart, R. Q. Snurr and O. K. Farha, *J. Am. Chem. Soc.*, 2022, **144**, 12212–12218.
22 S. Capelo-Aviles, M. de Fez-Febre, S. R. G. Balestra, J. Cabezas-Gimenez, R. Tomazini de Oliveira, S. Gallo II, A. Vidal-Ferran, J. Gonzalez-Cobos, V. Lillo, O. Fabelo, E. C. Escudero-Adan, L. R. Falvello, J. B. Parra, P. Rumori, G. Turnes Palomino, C. Palomino Cabello, S. Giancola, S. Calero and J. R. Galan-Mascaros, *Nat. Commun.*, 2025, **16**, 3243–3258.
23 Y. Qi, C. Xue, Y. Zhang, Y. Huang, H. Huang, L. Gan and H. Yang, *ACS Mater. Lett.*, 2025, **7**, 1488–1495.
24 N. Sun, X. Zhou, J. Liu, H. Yu, X. Si, F. Ding and Y. Sun, *J. Mater. Chem. A*, 2025, **13**, 9665–9672.
25 D.-H. Nam, O. Shekhah, A. Ozden, C. McCallum, F. Li, X. Wang, Y. Lum, T. Lee, J. Li, J. Wicks, A. Johnston, D. Sinton, M. Eddaoudi and E. H. Sargent, *Adv. Mater.*, 2022, **34**, 2207088.
26 Y. L. Li, N. Li, Z. B. Mei, J. R. Li, S. J. Yao, F. Yu, S. L. Li, J. M. Lin, J. Liu and Y. Q. Lan, *Chem. Sci.*, 2025, **16**, 11939–11948.
27 Y. Liang, H. Zhou, Y. Zhao, X. Liang, Z. Chen, M. Ji and M. Wang, *Chem. Sci.*, 2025, **16**, 15223–15230.
28 A. Pal, S. Suresh, A. Khan, L. H. Kuo, L. T. Chi, A. Ganguly, C. Y. Kao, M. K. Sharma, T. S. A. Wang, D. Y. Kang and Z. H. Lin, *Sci. Adv.*, 2025, **11**, eads4711.
29 Y.-Y. Tang, X. Luo, R.-Q. Xia, J. Luo, S.-K. Peng, Z.-N. Liu, Q. Gao, M. Xie, R.-J. Wei, G.-H. Ning and D. Li, *Angew. Chem., Int. Ed.*, 2024, **63**, e202408186.
30 K. Gupta and A. K. Patra, *ACS Sens.*, 2020, **5**, 1268–1272.
31 J. Wang, Y. Cheng, J. Zhou and W. Tang, *J. Mater. Chem. C*, 2021, **9**, 12086–12093.
32 S. Ghosh, R. Lipin, A. Ngoipala, N. Ruser, D. M. Venturi, A. Rana, M. Vandichel and S. Biswas, *Inorg. Chem.*, 2023, **62**, 14632–14646.
33 J. Y. M. Chan, E. O. Shehayeb, D. L. Pennington, C. H. Hendon and K. A. Mirica, *J. Am. Chem. Soc.*, 2025, **147**, 29003–29012.
34 Y. Shen, A. Tissot and C. Serre, *Chem. Sci.*, 2022, **13**, 13978–14007.
35 Z. Han, K. Y. Wang, R. R. Liang, Y. Guo, Y. Yang, M. Wang, Y. Mao, J. Huo, W. Shi and H. C. Zhou, *J. Am. Chem. Soc.*, 2025, **147**, 3866–3873.
36 M. Ran, Y. Liu, L. Feng, J. Ning, J. Li and X. Dou, *ACS Appl. Nano Mater.*, 2025, **8**, 8231–8240.

37 P. Horcajada, T. Chalati, C. Serre, B. Gillet, C. Sebrie, T. Baati, J. F. Eubank, D. Heurtaux, P. Clayette, C. Kreuz, J. S. Chang, Y. K. Hwang, V. Marsaud, P. N. Bories, L. Cynober, S. Gil, G. Ferey, P. Couvreur and R. Gref, *Nat. Mater.*, 2010, **9**, 172–178.

38 X.-X. Zeng, J.-S. Lu, D.-W. Ma, Y.-T. Huang, L. Chen, G. Wang, Q. Chen and N. Lin, *Rare Met.*, 2024, **43**, 4867–4883.

39 J. R. Li, R. J. Kuppler and H. C. Zhou, *Chem. Soc. Rev.*, 2009, **38**, 1477–1504.

40 Z. Bao, G. Chang, H. Xing, R. Krishna, Q. Ren and B. Chen, *Energy Environ. Sci.*, 2016, **9**, 3612–3641.

41 H. Li, K. Wang, Y. Sun, C. T. Lollar, J. Li and H.-C. Zhou, *Mater. Today*, 2018, **21**, 108–121.

42 R.-B. Lin, S. Xiang, W. Zhou and B. Chen, *Chem*, 2020, **6**, 337–363.

43 L. Yang, S. Qian, X. Wang, X. Cui, B. Chen and H. Xing, *Chem. Soc. Rev.*, 2020, **49**, 5359–5406.

44 L. Yang, P. Zhang, J. Cui, X. Cui and H. Xing, *Angew. Chem., Int. Ed.*, 2024, **63**, e202414503.

45 C. Gücüyener, J. van den Bergh, J. Gascon and F. Kapteijn, *J. Am. Chem. Soc.*, 2010, **132**, 17704–17706.

46 P. Q. Liao, W. X. Zhang, J. P. Zhang and X. M. Chen, *Nat. Commun.*, 2015, **6**, 8697.

47 H. G. Hao, Y. F. Zhao, D. M. Chen, J. M. Yu, K. Tan, S. Ma, Y. Chabal, Z. M. Zhang, J. M. Dou, Z. H. Xiao, G. Day, H. C. Zhou and T. B. Lu, *Angew. Chem., Int. Ed.*, 2018, **57**, 16067–16071.

48 Y. Chen, Z. Qiao, H. Wu, D. Lv, R. Shi, Q. Xia, J. Zhou and Z. Li, *Chem. Eng. Sci.*, 2018, **175**, 110–117.

49 Y. Han, L. Meng, Y. Liu, H. Li, Z. Ji, Y. Zhou, M. Wu and Z. Han, *Sep. Purif. Technol.*, 2023, **315**, 123642.

50 L. Li, R. B. Lin, R. Krishna, H. Li, S. Xiang, H. Wu, J. Li, W. Zhou and B. Chen, *Science*, 2018, **362**, 443–446.

51 M. Li, L. Yin, S. Li, J. Miao, Z. Wang and H. Wang, *Inorg. Chem.*, 2025, **64**, 12440–12445.

52 S. M. Wang, M. Shivanna, S. T. Zheng, T. Pham, K. A. Forrest, Q. Y. Yang, Q. Guan, B. Space, S. Kitagawa and M. J. Zaworotko, *J. Am. Chem. Soc.*, 2024, **146**, 4153–4161.

53 Y. Wang, F. Zhang, Y. Yang, X. Wang, L. Li, J. Li and J. Yang, *J. Colloid Interface Sci.*, 2025, **687**, 439–448.

54 F. Xie, J. Liu, W. Graham, S. Ullah, E. M. Cedeño Morales, K. Tan, T. Thonhauser, H. Wang and J. Li, *Chem. Eng. J.*, 2023, **473**, 145096.

55 Y. Ye, Y. Xie, Y. Shi, L. Gong, J. Phipps, A. M. Al-Enizi, A. Nafady, B. Chen and S. Ma, *Angew. Chem., Int. Ed.*, 2023, **62**, e202302564.

56 L. P. Zhang, G. W. Guan, Y. T. Li, H. R. Liu, S. T. Zheng, Y. Jiang, R. Bai and Q. Y. Yang, *Small*, 2024, **20**, e2402382.

57 Z. Xu, X. Xiong, J. Xiong, R. Krishna, L. Li, Y. Fan, F. Luo and B. Chen, *Nat. Commun.*, 2020, **11**, 3163.

58 B. Zhu, J. W. Cao, S. Mukherjee, T. Pham, T. Zhang, T. Wang, X. Jiang, K. A. Forrest, M. J. Zaworotko and K. J. Chen, *J. Am. Chem. Soc.*, 2021, **143**, 1485–1492.

59 G. D. Wang, Y. Z. Li, W. J. Shi, L. Hou, Y. Y. Wang and Z. Zhu, *Angew. Chem., Int. Ed.*, 2022, **61**, e202205427.

60 J. Liu, H. Wang and J. Li, *Chem. Sci.*, 2023, **14**, 5912–5917.

61 Z. Ji, Q. Li, Y. Zhou, R. Krishna, M. Hong and M. Wu, *Angew. Chem., Int. Ed.*, 2024, **63**, e202411175.

62 X. Jiang, Y. Wang, H. Wang, L. Cheng, J. W. Cao, J. B. Wang, R. Yang, D. H. Zhang, R. Y. Zhang, X. B. Yang, S. H. Wang, Q. Y. Zhang and K. J. Chen, *Nat. Commun.*, 2025, **16**, 694–704.

63 Q. Ding, Z. Zhang, Y. Liu, K. Chai, R. Krishna and S. Zhang, *Angew. Chem., Int. Ed.*, 2022, **61**, e202208134.

64 Y. N. Ma, T. L. Liu, W. H. Zhang, C. H. He and D. X. Xue, *Angew. Chem., Int. Ed.*, 2025, **64**, e202513208.

65 O. Delgado Friedrichs, M. O'Keeffe and O. M. Yaghi, *Acta Crystallogr., Sect. A: Found. Adv.*, 2003, **59**, 515–525.

66 N. W. Ockwig, O. Delgado-Friedrichs, M. O'Keeffe and O. M. Yaghi, *Acc. Chem. Res.*, 2005, **38**, 176–182.

67 O. Delgado-Friedrichs, M. O'Keeffe and O. M. Yaghi, *Acta Crystallogr., Sect. A: Found. Adv.*, 2006, **62**, 350–355.

68 J. Kim and W. Choe, *Chem*, 2022, **8**, 617–631.

69 P. M. Bhatt, V. Guillerm, S. J. Datta, A. Shkurenko and M. Eddaoudi, *Chem*, 2020, **6**, 1613–1633.

70 M. O'Keeffe, M. A. Peskov, S. J. Ramsden and O. M. Yaghi, *Acc. Chem. Res.*, 2008, **41**, 1782–1789.

71 Y. Ye, Z. Ma, R. B. Lin, R. Krishna, W. Zhou, Q. Lin, Z. Zhang, S. Xiang and B. Chen, *J. Am. Chem. Soc.*, 2019, **141**, 4130–4136.

72 L. Liu, Z. Yao, Y. Ye, Y. Yang, Q. Lin, Z. Zhang, M. O'Keeffe and S. Xiang, *J. Am. Chem. Soc.*, 2020, **142**, 9258–9266.

73 A. N. Hong, H. Yang, X. Bu and P. Feng, *EnergyChem*, 2022, **4**, 100080.

74 X. Mu, Y. Xue, M. Hu, P. Zhang, Y. Wang, H. Li, S. Li and Q. Zhai, *Chin. Chem. Lett.*, 2023, **34**, 107296.

75 Y. Zhang, Y. Han, B. Luan, L. Wang, W. Yang, Y. Jiang, T. Ben, Y. He and B. Chen, *J. Am. Chem. Soc.*, 2024, **146**, 17220–17229.

76 Y. Z. Hao, K. Shao, X. Zhang, Y. H. Yu, D. Liu, H. M. Wen, Y. Cui, B. Li, B. Chen and G. Qian, *J. Am. Chem. Soc.*, 2025, **147**, 11257–11266.

77 W. Wang, Y. Chen, K. X. Phan, Z. Jia, Y. Xiao, X. Bu and P. Feng, *J. Am. Chem. Soc.*, 2025, **147**, 31239–31248.

78 Y. W. Chen, Z. W. Qiao, H. X. Wu, D. F. Lv, R. F. Shi, Q. B. Xia, J. Zhou and Z. Li, *Chem. Eng. Sci.*, 2018, **175**, 110–117.

79 H. M. Wen, C. Yu, M. Liu, C. Lin, B. Zhao, H. Wu, W. Zhou, B. Chen and J. Hu, *Angew. Chem., Int. Ed.*, 2023, **62**, e202309108.

80 X. W. Gu, J. X. Wang, E. Wu, H. Wu, W. Zhou, G. Qian, B. Chen and B. Li, *J. Am. Chem. Soc.*, 2022, **144**, 2614–2623.

81 J. W. Cao, S. Mukherjee, T. Pham, Y. Wang, T. Wang, T. Zhang, X. Jiang, H. J. Tang, K. A. Forrest, B. Space, M. J. Zaworotko and K. J. Chen, *Nat. Commun.*, 2021, **12**, 6507–6515.

82 H. Zeng, X. J. Xie, M. Xie, Y. L. Huang, D. Luo, T. Wang, Y. Zhao, W. Lu and D. Li, *J. Am. Chem. Soc.*, 2019, **141**, 20390–20396.

83 Q. L. Hong, W. J. Wang, S. M. Chen, K. Chen, M. Liu, H. X. Zhang and J. Zhang, *Chem. Mater.*, 2022, **34**, 307–313.

84 M. H. Yu, H. Fang, H. L. Huang, M. Zhao, Z. Y. Su, H. X. Nie, Z. Chang and T. L. Hu, *Small*, 2023, **19**, 2300821.

85 Y. Wang, C. Hao, W. Fan, M. Fu, X. Wang, Z. Wang, L. Zhu, Y. Li, X. Lu, F. Dai, Z. Kang, R. Wang, W. Guo, S. Hu and D. Sun, *Angew. Chem., Int. Ed.*, 2021, **60**, 11350–11358.

86 G. D. Wang, Y. Z. Li, W. J. Shi, L. Hou, Y. Y. Wang and Z. Zhu, *Angew. Chem., Int. Ed.*, 2023, **62**, e202311654.

87 S. Q. Yang, F. Z. Sun, P. Liu, L. Li, R. Krishna, Y. H. Zhang, Q. Li, L. Zhou and T. L. Hu, *ACS Appl. Mater. Interfaces*, 2021, **13**, 962–969.

88 G. D. Wang, Y. Z. Li, H. Zeng, L. Hou, W. G. Lu and D. Li, *Adv. Funct. Mater.*, 2025, **35**, 2504916.

89 F. Xie, J. Q. Liu, W. Graham, S. Ullah, E. M. C. Morale, K. Tan, T. Thonhauser, H. Wang and J. Li, *Chem. Eng. J.*, 2023, **473**, 145096.

90 (*a*) CCDC 2482490: Experimental Crystal Structure Determination, 2025, DOI: 10.5517/ccdc.csd.cc2pb7bm; (*b*) CCDC 2482491: Experimental Crystal Structure Determination, 2025, DOI: 10.5517/ccdc.csd.cc2pb7cn.